Journal of Environmental Chemical Engineering 5 (2017) 292–302

Contents lists available at ScienceDirect

Journal of Environmental Chemical Engineering

journal homepage: www.elsevier.com/locate/jece

Research Paper

Monolithic reactor for VOCs abatement: Influence of non-uniformity in the coating

M. Laura Rodríguez[a,*], Luis E. Cadús[a], Daniel O. Borio[b]

[a] INTEQUI/UNSL-CONICET, Chacabuco y Pedernera, 5200 San Luis, Argentina
[b] PLAPIQUI/UNS-CONICET, Camino La Carrindanga km. 7, 8000, Bahía Blanca, Argentina

ARTICLE INFO

Article history:
Received 16 September 2016
Received in revised form 18 November 2016
Accepted 25 November 2016
Available online 27 November 2016

Keywords:
Structured reactor
VOCs catalytic combustion
Diffusion-reaction model
Non-uniform coating
Thermal effects

ABSTRACT

This article presents a theoretical study of the catalytic mineralisation of ethanol via acetaldehyde over manganese – copper mixed oxide catalyst deposited on a monolith reactor. The steady-state operation of the monolith reactor is represented by means a heterogeneous, one-dimensional, adiabatic model, which accounts for external (gas-solid) resistances to mass and heat transfer and internal resistances to mass transfer inside the catalytic coating (washcoat).

The effect of catalyst accumulation at the corners of a square section channel is analysed. Under the operating conditions considered, the diffusional resistances have a significant effect on the effective rate of removal of Volatile Organic Compounds and cannot be neglected. Non-uniform coating causes a considerable deterioration of the averaged effectiveness factors of the two reactions under consideration and lower temperatures along the reactor are found. These lower temperatures, together with lower temperature drops over the external film cause additional negative impacts on the Volatile Organic Compounds conversion. The decrease in the reactor performance, caused by the catalyst accumulation, is magnified as the feed concentration rises. Consequently, higher feed temperatures and/or lower space velocities are necessary to ensure the complete destruction of the volatile organic compounds involved (ethanol and acetaldehyde).

1. Introduction

Volatile Organic Compounds (VOCs) are considered to be hazardous air pollutants because of their many harmful effects on health and the environment [1]. More and more, strict and precise global standards are being established to control the emissions of these dangerous pollutants [2,3]. The European Commission sets an Emission Limit Value (ELV) of 20 mg C/m^3 for streams discharged into the atmosphere [2].

There are several techniques available to control VOCs emission (destruction based and recovery based) with many advantages and limitations [1,4]. Adsorption and thermal oxidation lie among the most used [1]. In the former, VOCs are adsorbed in a solid phase, e.g., activated carbon, and then need to be released from it, which requires energy. Additionally, and depending on the composition of the VOC stream, undesirable side reactions may occur in the adsorption bed [5]. A typical end-pipe VOC emission is characterised by a very low concentration of organic species (in the range of 50–2000 ppm) and large gas flowrates (1700–17000 m^3/h) [6]. For these operative conditions, thermal oxidation is generally not suitable. High concentrations of VOCs are required to obtain a sufficient calorific value to sustain operating temperatures and stable combustion conditions. If VOC concentrations are low, then auxiliary fuel requirements may be substantial and add to the operating costs. In addition, flame temperatures in thermal incinerators are generally at a level at which NOx emissions become significant, and depending on the composition of the VOCs and the nature of the auxiliary fuel, particulate emissions may occur [1,4,5].

Catalytic oxidation appears as a low energy consumption technology [1]. In this process the VOC stream is generally preheated (at a minimum operating temperature) and fed into a reactor that contains a structured catalyst [5,7]. This method is particularly suitable for the treatment of low concentrations of VOCs (e.g., ppm level) [5].

* Corresponding author.
E-mail address: mlrodri@unsl.edu.al (M. L. Rodríguez).

http://dx.doi.org/10.1016/j.jece.2016.11.036
2213-3437/

Nomenclature

a_v	Gas-solid interfacial area, m^2/m^3
A	Value of the Cartesian coordinate position of the centre of a circumference of R_{NC} radius, mm (see Fig. 1)
b	Channel width = height, mm
C_j	Concentration of j component, mol_j/m^3 or mg C/m^3
$C_{s,j}$	Concentration of j component in the solid phase, mol_j/m^3 or mg C/m^3
$C^s_{s,j}$	Concentration of j component at surface of the solid phase, mol_j/m^3 or mg C/m^3
C_{pj}	Heat capacity of j component, J/mol_j K
CN	Channels number, dimensionless
$D_{e,j}$	Effective diffusion coefficient for j component, m^2/s
E_i	Activation energy of i reaction, J/mol
ELV	Emission Limit Value, 20 mg C/m^3 (total VOC emissions at standard conditions)
G	Specific mass flow per channel, kg/(m^2 h)
$GHSV$	Gas-hourly space velocity, 1/h
h_e	Convective heat transfer coefficient, J/(s m^2 K)
$k_{g,j}$	Convective mass transfer coefficient from gas to solid interface, m^3f/(m^2s)
$k_{ref,1}$	Kinetic constant of reaction 1, 1/s
$k_{ref,2}$	Kinetic constant of reaction 2, mol/(m^3 s)
K_{cj}	Adsorption constant of j component, m^3/mol
L	Channel length, m
$LHHW$	Langmuir-Hinshelwood Hougen-Watson
m_w	Catalyst mass, g
P	Pressure, atm
Q_0	Volumetric feed flow rate, Nm^3/h
r_i	Reaction rate of i reaction, i = 1,2, mol/(m^3_w s)
r_i^B	Reaction rate of i reaction at gas phase, i = 1,2, mol/(m^3_w s)
r_i^{eff}	Effective reaction rate of i reaction, i = 1,2, mol/(m^3_w s)
r_i^S	Reaction rate of i reaction at gas-solid inteface, i = 1,2, mol/(m^3_w s)
R	Universal gas constant, J/(mol K)
R_{NC}	Normalized curvature radius, dimensionless
s_k	k slice
T	Gas phase temperature, °C
T^S	Solid phase temperature, °C
u_s	Average gas velocity, m/s
V_g	Gas volume, m^3
V_w	Washcoat volume, m^3
w_k	Weight factor for k slice, dimensionless
x	Transversal coordinate, m
z	Axial coordinate, m

Compounds

C	Carbon
C_2H_5OH	Ethanol
C_2H_4O	Acetaldehyde
CO	Carbon monoxide
CO_2	Carbon dioxide
H_2O	Water
N_2	Nitrogen
NOx	Nitrogen oxides
O_2	Oxygen
VOC	Volatile organic compound

Greek letters

δ_k	Washcoat thickness of k slice, μm
$\overline{\delta}_w$	Average washcoat thickness, μm
ε_i	Extent of i reaction, mol/h
ΔC_{VOC}	Maximum difference in VOC outlet concentration between two different catalyst distribution (R_{NC} = 0 and 0.5), mg C/m^3
$\Delta H^o_{r_i}$	Heat of i reaction at standard conditions, J/mol
ΔH_{r_i}	Heat of i reaction, J/mol
ΔT_{ad}	Adiabatic temperature gradient, °C
ΔT_g	Total temperature gradient (inlet-outlet) in the gas phase, °C
$\Delta T_{s\text{-}g}$	Interfacial temperature gradient, °C
$\Delta T_{s\text{-}g,max}$	Maximum interfacial temperature gradient, °C
Δz	Differential increment in z axial coordinate, m
$\eta_{i,k}$	Internal effectiveness factor of i reaction in k silce, dimensionless
$\overline{\eta}_i$	Average internal effectiveness factor of i reaction, dimensionless
ρ_g	Gas density, kg/m^3
ρ_w	Washcoat density, kg/m^3

Subscripts

Ac	Acetaldehyde
Et	Ethanol
i	i reaction
k	k slice
max	Maximum
ref	Reference
s-g	Solid-gas interface
VOC	Volatile organic compound
w	Washcoat
0	At the axial coordinate z = 0

Superscripts

B	At bulk gas phase
eff	Effective
S	At solid surface
o	At standard condition

The monolithic catalyst consists of thousands of small parallel channels of about 1 mm hydraulic diameter, with ceramic or metallic walls between them. The catalytically active material is deposited on the walls forming a porous layer, typically 10–100 μm thick [8].

Its outstanding performance is due to its high specific area (more than 4000 m^2/m^3), low pressure drop, especially if compared with packed bed reactors, and finally, to its excellent mechanical and thermal resistances [9,10].

Considerable efforts have been directed towards obtaining suitable catalysts for VOCs' catalytic oxidation [7,11]. It has been demonstrated that Mn-Cu mixed oxide catalysts are highly active at moderate temperatures for the catalytic oxidation of a wide variety of VOCs [12]. This catalyst has been successfully deposited by impregnation on ceramic monoliths [13].

When the monolith is operated at low temperature, the catalytic reactions are slow and limit the overall reactant conversion. At higher temperatures, mass transfer processes have a much weaker dependence on temperature than reaction rates, and become rate-limiting [8]. Modern catalysts are very active and, even thin washcoats, can show large concentration gradients at higher temperature [14]. The washcoat often has a non-uniform thickness because the material tends to accumulate on corners. Thus, while the thickness may be only 10 μm at the side, it may be up to 150 μm thick on the corners [15]. Such a non-uniform shape of the washcoat naturally affects the effectiveness factor behaviour.

Hence, a correct analysis of the mass transfer resistances is important to model the performance of monolithic reactors accurately [15,16]. The effect of mass transfer limitations in monolith catalysts with rounded corners has been extensively studied [8,14–22].

Chou and Stewart [17] were among the first to address the influence of the washcoat geometry on the effectiveness factor. They applied a 2D reaction-diffusion model to investigate this effect for a first order isothermal reaction. However, the results were not extended to include reactor simulations. Holmgren and Andersson [8] performed experiments for CO oxidation and used a 3D CFD simulations to study mass transfer in square monolith channels with rounded corners with the aim of obtaining an accurate Sherwood expression. According to the authors, the high mass transfer rates found in experimental measurements were higher than theoretical results due to the turbulence generated at the reactor inlet. Leung et al. [18] presented numerical solutions of diffusion with chemical reaction in a monolith washcoat for the oxidation of carbon monoxide and propane, and demonstrated that diffusion limitation could be significant at typical operating temperatures. They compared the 2D solution to a 1D approximation based on the generalized Thiele modulus approach. The solutions matched in the asymptotic regions of high and low Thiele modulus, and showed some differences in the intermediate region. In the case of multiple reactions, the method becomes computationally expensive. Kolaczkowski and Serbetcioglu [19] studied CO oxidation over noble-metal based catalyst systems. As Leung et al. [18], they also considered washcoat shapes that result from fillets in the corner of square channels, and demonstrated that both interphase mass and heat transfer and intraphase mass transfer are strongly affected by the catalyst accumulation in these corners. Papadias et al. [16] developed a simplified method to calculate the effectiveness factors in irregular geometries of washcoats. The method consists in sectioning the washcoat into particles (or fillets) and treating each particle in a 1D approach. This simplified method was compared with a rigorous 2D model for different kinds of kinetic expressions and geometrical shapes of the washcoat. In general, the simplified method gives a good a priori estimation of the effectiveness factor that can replace tedious and time-consuming finite element calculations in irregular shapes of washcoats. Hayes et al. [20], inquired the influence of washcoat and channel shape on the mass transfer and concluded that, for non-uniform washcoats, the Sherwood numbers and hence the mass transfer coefficient, vary along the gas solid interface. The authors found that washcoat thickness, channel radius, including its non-uniformity around the channel, and angular diffusion in the washcoat caused by variable thickness in non-symmetrical geometries are the three factors determining mass transfer rates. Hayes et al. [21,22], presented an extension of the method proposed to Papadias et al. [16] with the aim of improving the efficiency of the numerical solution for complex kinetics in which 1D problems need to be solved numerically. A 2D finite element monolith reactor model for catalytic oxidation of propane was proposed and used by Hayes et al. [23] to study external and internal heat transfer in ceramic monoliths. They found that both heat radiation and conduction affected the outlet temperature with axial conduction being more significant.

Mass transfer resistances in non-uniformly coated ceramic monoliths have been extensively studied under isothermal conditions. However, there is a lack of studies focused on simultaneous heat and mass-transfer limitations, which take place when the monoliths are being operated in the presence of strong heat effects.

The purpose of this paper is to present results of a theoretical study of the catalytic oxidation of ethanol over a Mn–Cu mixed oxide catalyst deposited on a monolith reactor. Through a rigorous evaluation of external (gas-solid) resistances to mass and heat transfer and internal resistances to mass transfer inside the washcoat, we analyse the behaviour of an adiabatic monolith considering a non-uniform catalytic material distribution on the channel walls. We also point out the influence of this non-uniformity on the outlet conversion and temperature profiles, for feed concentrations leading to significant heat effects.

The capacity of the monolith to accomplish VOC emission limit values is studied at operating conditions close to the industrial ones.

2. Mathematical model

The reactor feed consists in a stream of ethanol diluted in air. Channels of square section are impregnated with the Mn-Cu mixed oxide catalyst [12]. A scheme of the simulated monolithic reactor is shown in Fig. 1a. Fig. 1b illustrates the mass and heat transfer resistances considered in a differential control volume. Due to the symmetry of the channel it is enough to analyse only 1/8 of the total channel section, which has been subdivided into eight consecutive slices, from s_1 to s_8, which are considered as rectangular sections (1D sliced model [20]). In each rectangular section, local internal effectiveness factors for both reactions are calculated using a 1D flat plate model. Average internal effectiveness factors (η_1 and η_2) are calculated at each axial position. Mass and heat balances are solved for gas and solid phases along the axial position. The model accounts for external resistances to mass and heat transfer and internal resistances to mass transfer. The cross section of each slice varies with the normalized curvature radius (R_{NC}).

$R_{NC}=0$ indicates that no catalyst accumulation at the corners exists, i.e, the washcoat thickness is constant around the channel, while $R_{NC}>0$ represents an additional accumulation of catalytic material on the corners of the channel.

2.1. Model equations

A heterogeneous 1D mathematical model is proposed to simulate the adiabatic and steady state operation of the monolithic reactor, based on the following hypotheses:

(a) Fully developed laminar flow through the channels is assumed, leading to low pressure drops and nearly isobaric conditions.
(b) Heat losses to the surrounding are neglected.
(c) Axial dispersion of heat and mass is neglected (axial mass and heat Peclet numbers are much higher than 50) [24].
(d) Isothermal conditions in the catalyst layer are assumed from the evaluation of Biot [25] and Prater [19,26] numbers, both values are much lower than 1.
(e) Inside the channel the flow is unidirectional
(f) A single channel is assumed to be representative of the whole reactor: the flow distribution is uniform and the catalyst is equally distributed among the channels. There are no radial gradients of temperature and composition across the monolith [27].

The catalytic combustion of ethanol is evaluated by means of the kinetic model proposed by Campesi et al. [28]. Two reactions in series are considered: partial oxidation of ethanol to acetaldehyde and combustion of acetaldehyde (see Table 1).

Table 2 lists the kinetic parameters and the standard heats of reactions 1 and 2. Since there are two reactions involved, from the mass balances corresponding to ethanol and acetaldehyde it is possible to calculate the extent of reaction 1 (ε_1) and 2 (ε_2). The concentrations of the remaining species CO_2, O_2, N_2 and H_2O are

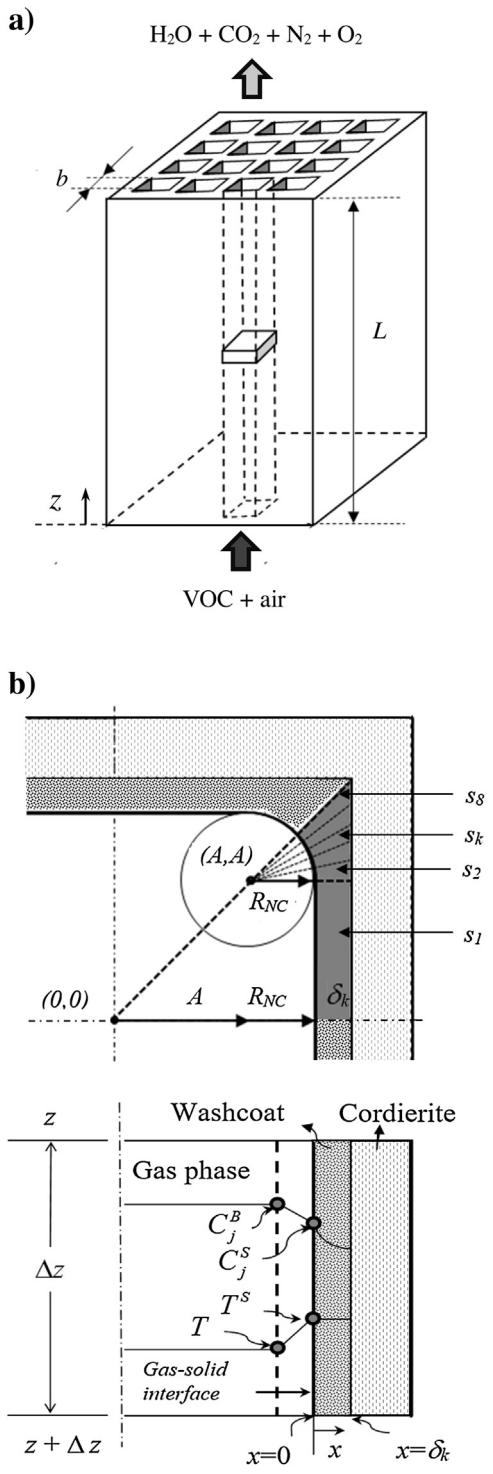

Fig. 1. a) Schematic representation of the monolithic reactor. b) Schematic detail of the transverse channel section and representation of the mass and heat transfer resistances considered in a differential control volume.

Table 1
Reaction system and kinetic expressions [28].

Reaction system	Kinetic expressions	
$C_2H_6O + (1/2)O_2 \rightarrow C_2H_4O + H_2O$	$r_1 = \frac{k_{ref,1}\exp[-(E_1/R)(1/T-1/T_{ref})]C_{Et}}{1+Kc_{Et}C_{Et}+Kc_{Ac}C_{Ac}}$	(1)
$C_2H_4O + (5/2)O_2 \rightarrow 2CO_2 + 2H_2O$	$r_2 = \frac{k_{ref,2}\exp[-(E_2/R)(1/T-1/T_{ref})]Kc_{Ac}C_{Ac}}{1+Kc_{Et}C_{Et}+Kc_{Ac}C_{Ac}}$	(2)

obtained from the molar balances as function of the parameters ε_1 and ε_2 [30].

Under the stated hypotheses, the reactor is represented by the following equations:

2.1.1. Gas phase

2.1.1.1. Mass balances.

$$\frac{dC_{Et}}{dz} = -\frac{V_w}{u_s V_g}\overline{\eta}_1 r_1^S \tag{3}$$

$$\frac{dC_{Ac}}{dz} = \frac{V_w}{u_s V_g}\left(\overline{\eta}_1 r_1^S - \overline{\eta}_2 r_2^S\right) \tag{4}$$

where:

$$\overline{\eta}_i = \sum_{k=1}^{k=8} w_k \eta_{i,k} \tag{5}$$

$$\eta_{i,k} = \frac{\int_0^{V_w} r_i(C_{s,Et}, C_{s,Ac})\,dV_w}{V_w r_i\left(C_{Et}^S, C_{Ac}^S\right)} = \frac{r_{i,k}^{eff}}{r_{i,k}^S} \tag{6}$$

for i = 1, 2; k = 1, 2, . . . , 8

Heat Balance

$$\frac{\frac{dT}{dz} = \frac{V_w}{u_s V_g}\eta_1 r_1^S(-\Delta H_{r_1}) + \eta_2 r_2^S(-\Delta H_{r_2})}{\sum_j Cp_j C_j} \tag{7}$$

with $j = C_2H_5OH$, C_2H_4O, CO_2, H_2O, N_2, O_2

Inlet conditions:

At z = 0:

$$C_{Et} = C_{0Et}, C_{Ac} = C_{0Ac}, \mathrm{T} = T_0 \tag{8}$$

2.1.2. Solid phase

Mass Balances (washcoat)

$$D_{e,Et}\frac{d^2C_{s,Et}}{dx^2} = -\frac{V_w}{V_g}r_1(C_{s,Et}, C_{s,Ac}) \tag{9}$$

$$D_{e,Ac}\frac{d^2C_{s,Ac}}{dx^2} = \frac{V_w}{V_g}\left(r_1(C_{s,Et}, C_{s,Ac}) - r_2(C_{s,Et}, C_{s,Ac})\right) \tag{10}$$

Boundary conditions:

At x = 0 (gas-solid interphase):

$$k_{g,j}\left(C_j - C_{s,j}^S\right) = -D_{e,j}\left(\frac{dC_{s,j}}{dx}\right)|_{x=0} \tag{11}$$

At $x = \delta_k$ (washcoat-cordierite surface):

$$\frac{dC_{s,j}}{dx} = 0 \tag{12}$$

with $j = C_2H_5OH$, C_2H_4O

2.1.3. Heat balance

$$a_v h_e\left(T - T^S\right) = \overline{\eta}_1 r_1^S(-\Delta H_{r_1}) + \overline{\eta}_2 r_2^S(-\Delta H_{r_2}) \tag{13}$$

For each slice, the local effectiveness factors for both reactions ($\eta_{1,k}$ and $\eta_{2,k}$) are calculated by Eq. (6). From these local values and

Table 2
Kinetic parameters [28] and standard heats of reactions.

Parameter	Optimal value and confidence interval
$k_{ref,1}$	$(1.81 \pm 0.3) \times 10^3$ 1/s
$k_{ref,2}$	$(1.81 \pm 0.26) \times 10^{-1}$ mol/(s m^3)
E_1	$(1.10 \pm 0.04) \times 10^5$ J/mol
E_2	$(1.69 \pm 0.09) \times 10^5$ J/mol
Kc_{Et}	~0
Kc_{Ac}	$(6.75 \pm 1.26) \times 10^2$ m^3/mol
$-\Delta H^o_{r1}$	1.73×10^5 J/mol
$-\Delta H^o_{r2}$	1.10×10^6 J/mol

the weight of each slice (w_k), the averaged effectiveness factors ($\overline{\eta}_1$ and $\overline{\eta}_2$) are obtained from Eq. (5). No diffusion is considered between slices. At each axial coordinate, a single temperature (T^S) is assumed for all the slices of the washcoat. The reaction rates in Eqs. (3)–(13) are evaluated at this temperature value for the solid phase.

At each axial position, the superficial velocity (u_s) (see Eqs. (3), (4) and (7)) is updated by means of the specific mass flow per channel (G, constant) and the gas density (ρ_g, variable). Thus,

$$u_s = \frac{G}{\rho_g} \tag{14}$$

Physical parameters of the catalyst (mean pore radius, washcoat porosity and tortuosity factor) [30] and physical and thermodynamic properties of the components [29,31] are extracted from the literature.

The convective mass and heat transfer coefficients are obtained from the Nusselt expression applicable to square-channel structured reactors proposed by Hawthorn [32]. Molecular binary diffusivity is calculated following Fuller, Schettler and Giddings's [33] semi empirical equation. Molecular mixed diffusivity for diluted systems, Knudsen diffusivity and effective diffusivity are calculated according to Froment and Bischoff's [34] guidelines.

2.2. Numerical solution

The differential equations for the gas phase are integrated using the Gear method [35]. The differential equations for the washcoat are discretized by means of second order finite differences, using a grid of equally spaced points in each slice. At each axial position, the nonlinear algebraic equations generated by the interior grid points of all of the slices are solved through a Quasi-Newton algorithm.

3. Results and discussion

3.1. Effect of curvature radius

The effect of the accumulation of catalytic material at the corners of the square section channels can be evaluated by varying the curvature radius (Fig. 1b), keeping invariant the total mass of catalyst (same transversal area of the catalytic coating), i.e, the mean washcoat thickness is constant ($\overline{\delta}_w = 30$ μm). The average thickness and the weight factor of each slice, δ_k and w_k, for the different values of R_{NC} considered, are listed in Tables 3 and 4, respectively.

Table 4
Weight factors of each slice.

R_{CN}	w_1	w_2	w_3	w_4	w_5	w_6	w_7	w_8
0	0.125	0.125	0.125	0.125	0.125	0.125	0.125	0.125
0.3	0.547	0.031	0.034	0.041	0.052	0.069	0.094	0.132
0.5	0.234	0.030	0.037	0.053	0.080	0.120	0.179	0.267
0.6	0.102	0.020	0.030	0.052	0.088	0.142	0.223	0.343

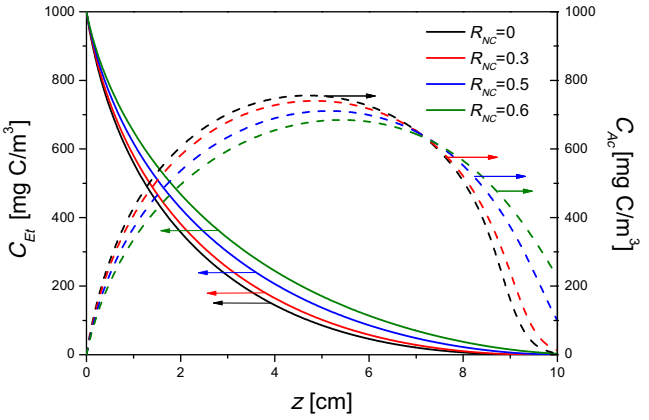

Fig. 2. Axial concentration profiles of ethanol and acetaldehyde, for the four curvature normalized radius (R_{NC} = 0, 0.3, 0.5 and 0.6). T_0 = 180 °C, C_{0Et} = 1000 mg C/m^3, $GHSV = 3.06 \times 10^5$ 1/h, = 30 μm, b = 1.115 mm, L = 10 cm.

Fig. 2 shows axial concentration profiles of ethanol and acetaldehyde for different R_{NC} values. The feed conditions and the remaining design parameters are kept invariant. Table 5 lists the geometrical parameters and operative conditions employed in the simulations. *GHSV* is calculated as the ratio between the volumetric flow rate at standard conditions and the total volume of the catalyst.

The maxima observed in the concentration profile of acetaldehyde correspond to a typical behaviour of an intermediate component (see Eqs. (1)–(2)). As the accumulation of catalytic material at the corners is more significant (higher values of R_{NC}), both, the ethanol and acetaldehyde consumptions decrease, leading to an incomplete VOC abatement. For $R_{NC} \geq 0.5$, the Emission Limit Value of VOC (*ELV* = 20 mg C/m^3) has been exceeded (see Table 6).

Fig. 3 shows the corresponding profiles of gas and solid temperatures for three of the curvature radius shown in Fig. 2a (R_{NC} = 0, 0.5 and 0.6). Non-uniform coating distributions cause lower temperature rises in the monolith (see the values of ΔTg in Table 6), because of the poorer effective reaction rates. The heat generation rates decrease and low average temperatures along the reactor length occur. The gas-solid temperature gradients (Fig. 4) are also affected by the catalyst distribution. In fact, the maximum interfacial temperature gradient is around 3.2 °C for the idealized catalyst distribution (R_{NC} = 0) and falls to 1.9 °C for R_{NC} = 0.6. It is

Table 3
Thickness of the slices.

R_{CN}	δ_1 (μm)	δ_2 (μm)	δ_3 (μm)	δ_4 (μm)	δ_5 (μm)	δ_6 (μm)	δ_7 (μm)	δ_8 (μm)
0	30	30	30	30	30	30	30	30
0.3	24.34	24.95	27.41	32.50	40.56	52.21	68.41	90.74
0.5	14.44	15.37	19.14	26.92	39.26	57.08	81.87	116.05
0.6	7.72	8.80	13.20	22.29	36.70	57.49	86.43	126.32

Table 5
Operative and geometrical parameters.

Parameter	Value
Channel length, L	0.10 m
Channel width = height, b	1115 μm
Cell density	400 cpsi
Channels number, CN	8444
Monolithic material	cordierite ($2MgO{\cdot}2Al_2O_3{\cdot}5SiO_2$)
Support	Nyacol
Catalytic material	Mn − Cu
Average washcoat thickness, $\overline{\delta}_w$	30 μm
Washcoat density, ρ_w	4030 kg/m^3
Washcoat mass, m_w	443 g
Inlet temperature, T_0	180 °C
Pressure, P	1 atm
Volumetric feed flow rate, Q_0	33.6 m^3/h
Gas-hourly space velocity, $GHSV$	3.06×10^5 1/h
Inlet VOC concentration, C_{0Et}	1000 mg C/m^3

important to note that despite the gas-solid specific area (a_v) exhibits a slight decrease as R_{NC} increases (see Table 6), this effect is not significant and the temperature drop over the film is dominated by the behaviour of the internal mass transfer resistances.

Fig. 5 presents curves of the effective reaction rates for reactions 1 and 2 (r_1^{eff} and r_2^{eff}), for two of the curvature radius analysed previously ($R_{NC}=0$ and $R_{NC}=0.6$). It is clear that the ethanol consumption rate (r_1^{eff}) deteriorates in the first section of the channels ($z<2.5$ cm) when R_{CN} increases. The reduction in the acetaldehyde consumption rate (r_2^{eff}) is much more pronounced, particularly in the second half of the reactor length. The curve of r_2^{eff} corresponding to $R_{NC}=0$ shows a well-defined maximum, located near the axial position of the maximum observed in the temperature drop over the film (Fig. 4, curve for $R_{CN}=0$). This is reasonable, because the total heat generation rate is dominated by the heat released in the second reaction, much more exothermic than r_1 (compare the values of $-\Delta H^o_{r_1}$ and $-\Delta H^o_{r_2}$ in Table 2). At the reactor outlet ($z=10$ cm), r_2^{eff} corresponding to $R_{NC}=0$ is close to zero, due to the conversion of acetaldehyde is practically complete. Conversely, curve of r_2^{eff} corresponding to $R_{NC}=0.6$ presents its maximum value at the reactor outlet, which is consistent with a condition of incomplete VOC depletion (see Fig. 2).

The reduction observed in the effective reaction rates is directly related to the behaviour of the averaged internal effectiveness factors ($\overline{\eta}_1$ and $\overline{\eta}_2$). The averaged internal effectiveness factor of i reaction ($\overline{\eta}_i$) is obtained as the weighted average of the local effectiveness factor for i reaction in k slice ($\eta_{i,k}$) multiplied by the weight factor of each slice (w_k) (see Eq. (5)).

The average internal effectiveness factors of reaction 1 ($\overline{\eta}_1$) for the four R_{NC} values are presented in Fig. 6a. A non-monotonous behaviour is registered, with a climb in the first quarter of the reactor length, achieving then a plateau zone and finally a decrease in the last quarter of the reactor length. This behaviour is associated with the kinetic expression for reaction 1 (LHHW type) which has been reported in the literature [34,36]. The significant decline observed in the averaged effectiveness factor as the non-uniformity of the coating increases is consistent with the shift to the right of the ethanol concentration profiles shown in Fig. 2 for the higher R_{CN} values. Fig. 6b shows the corresponding axial

Table 6
Operative and geometrical parameters for the conditions of Fig. 2.

R_{NC}	$C_{VOC,z=L}$ [mg C/m^3]	ΔT_g [° C]	a_v [m^2$_w$/m^3$_w$]	$\Delta T_{max,s\text{-}g}$ [° C]
0	4.5	45.8	32411.50	3.2
0.3.	13.2	45.5	30553.97	3.0
0.5	102.6	44.1	29692.14	2.4
0.6	228.7	39.3	29370.00	1.9

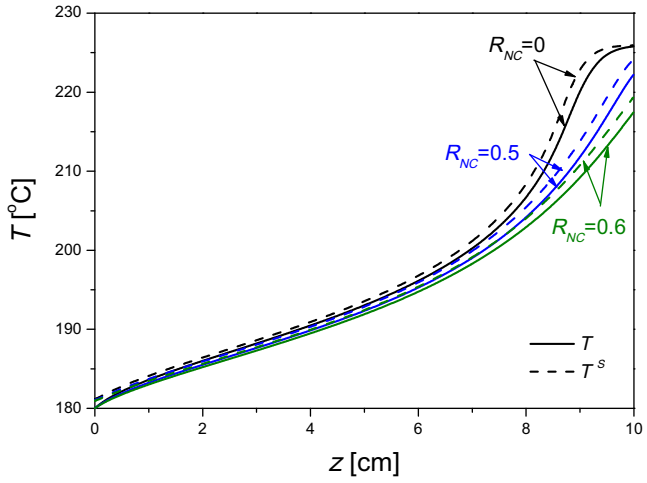

Fig. 3. Axial temperatures profiles in the gas (continuous line) and solid (dashed lines) phases for $R_{NC}=0$, 0.5 and 0.6, for the same conditions of Fig. 2.

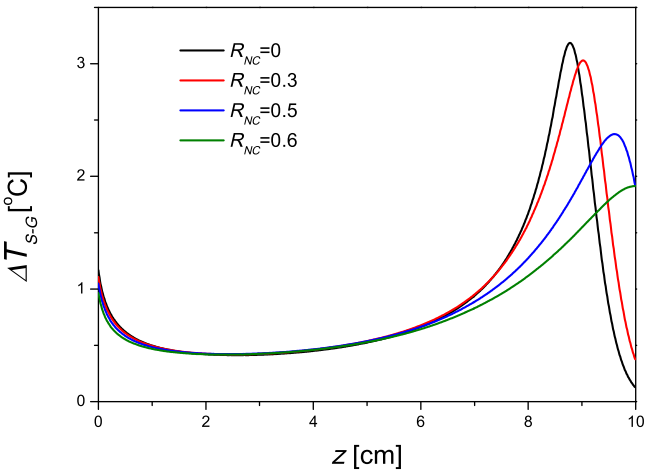

Fig. 4. Axial profiles of temperature drop over the film, for the four curvature normalized radius ($R_{NC}=0$, 0.3, 0.5 and 0.6) for the same conditions of Fig. 2.

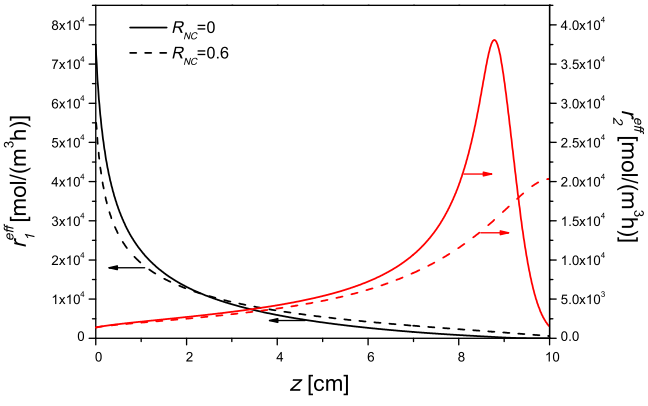

Fig. 5. Axial profiles of effective reaction rate 1 (r_1^{eff}) (left ordinate axis) for $R_{NC}=0$ and 0.6. Axial profiles of effective reaction rate 2 (r_2^{eff}) (right ordinate axis) for $R_{NC}=0$ and 0.6, for the conditions of Fig. 2.

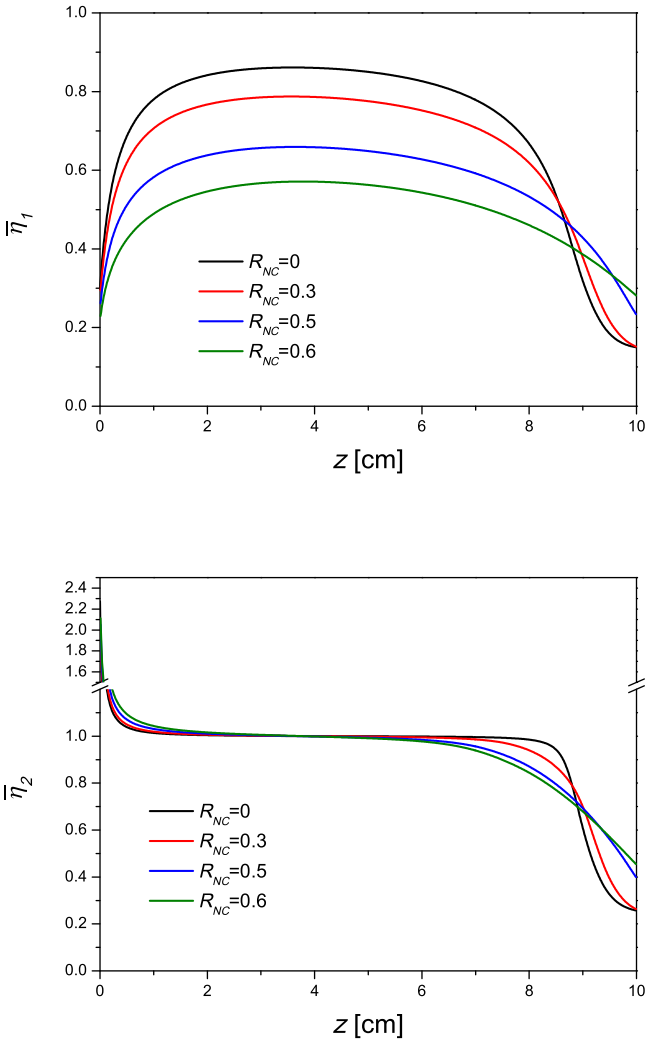

Fig. 6. a) Axial profiles of average internal effectiveness factor of reaction 1 ($\overline{\eta}_1$), b) Axial profiles of average internal effectiveness factor of reaction 2 ($\overline{\eta}_2$) for the conditions of Fig. 2.

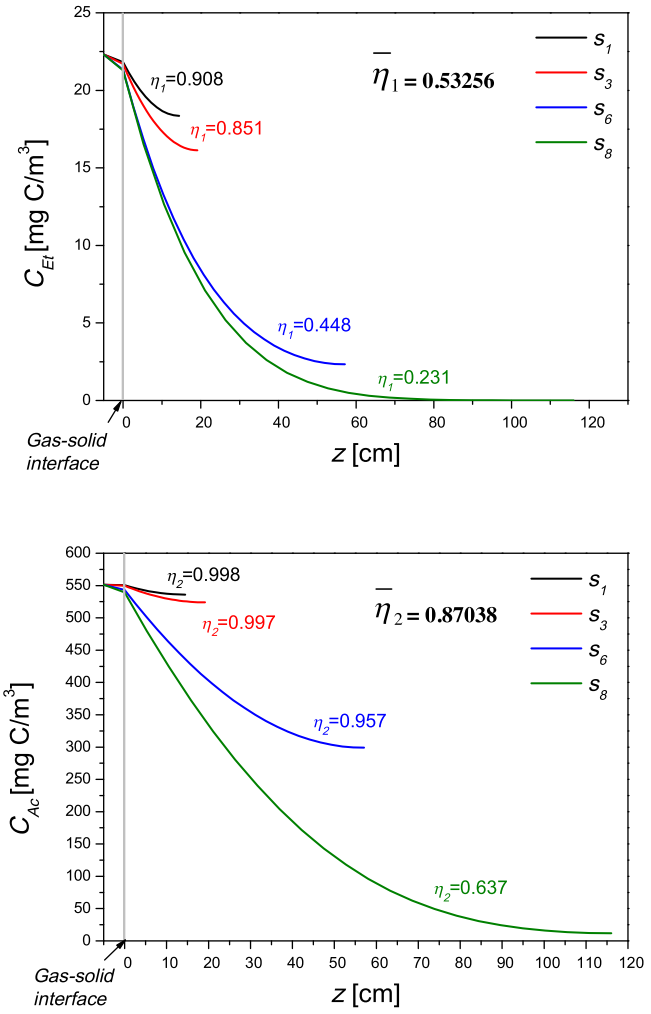

Fig. 7. a) Ethanol concentration cross-section profiles for R_{CN} = 0.5 at z = 8 cm, b) acetaldehyde concentration cross-section profiles for R_{CN} = 0.5 at z = 8 cm, for the conditions of Fig. 2.

profiles to the averaged internal effectiveness factor of reaction 2 ($\overline{\eta}_2$), defined as the ratio between r_2^{eff} and r_2^S. Close to the reactor inlet, where acetaldehyde is mainly generated (see Fig. 2) effectiveness factors are higher than one, because the concentration of acetaldehyde inside the washcoat is higher than that of the surface; an analogous behaviour is exhibited by the reaction rate, i.e., $r_2^{eff} > r_2^S$ which has been reported previously for a uniform washcoat [36]. This tendency is more pronounced as the non-uniformity of the washcoat increases (higher R_{CN}), because of influence of the thicker slices near the corner of the channel. In contrast, at the reactor outlet, the acetaldehyde is being mainly consumed and $\overline{\eta}_2$ is less than 1. In this zone of the reactor the effectiveness factor values drop for higher R_{CN} values, which correspond with the delayed acetaldehyde consumption observed in Fig. 2 in the last 30% of the channel length. In the reactor core, $\overline{\eta}_2$ presents a plateau with a value close to 1, due to for high concentration of acetaldehyde reaction 2 behaves approximately as a zero order reaction (see Eq. (2)).

Fig. 7a and b shows ethanol and acetaldehyde concentration cross-section profiles for a given curvature radius (R_{CN} = 0.5), a fixed axial position (z = 8 cm) and four different slices of the 1/8 washcoat area (s_1, s_3, s_6 and s_8). Fig. 7a illustrates that more pronounced ethanol concentration gradients occur for the slices near the corner (s_6 and s_8) due to the accumulation of catalytic material. As a consequence, the local internal effectiveness factor for reaction 1 ($\eta_{1,k}$) decrease notoriously, reaching a low value of 0.231 in the thickest slice (s_8), which has a thickness of 116 μm (see Table 4). For R_{CN} = 0.5, the weight factors of the two slices near the corner almost reach the 45% of the cross-section area (w_7 = 0.179 and w_8 = 0.267), which strongly influence the averaged internal effectiveness factor of reaction 1 ($\overline{\eta}_1$ = 0.533) (see Fig. 6a for R_{CN} = 0.5 at z = 8 cm). An analogous behaviour is observed for the acetaldehyde concentration cross-section profiles in the four selected slices, as shown in Fig. 7b.

Fig. 8a shows the acetaldehyde concentration cross-section profiles for R_{CN} = 0.5 at an axial position near the reactor inlet (z = 0.001 cm). In this axial position the profiles are growing into the catalytic coating, because $r_1 > r_2$ (acetaldehyde is mainly produced). As in the previous case, the higher concentration gradients are found in the thicker slices; however, at this axial position the acetaldehyde is diffusing from the core of the washcoat to the surface. The corresponding cross-section profiles of reaction rate r_2 are shown in Fig. 8b. It is clear that r_2 increases towards the interior of the washcoat, which is consistent with the values of the local effectiveness factors reported in Fig. 8a ($\eta_2 > 1$).

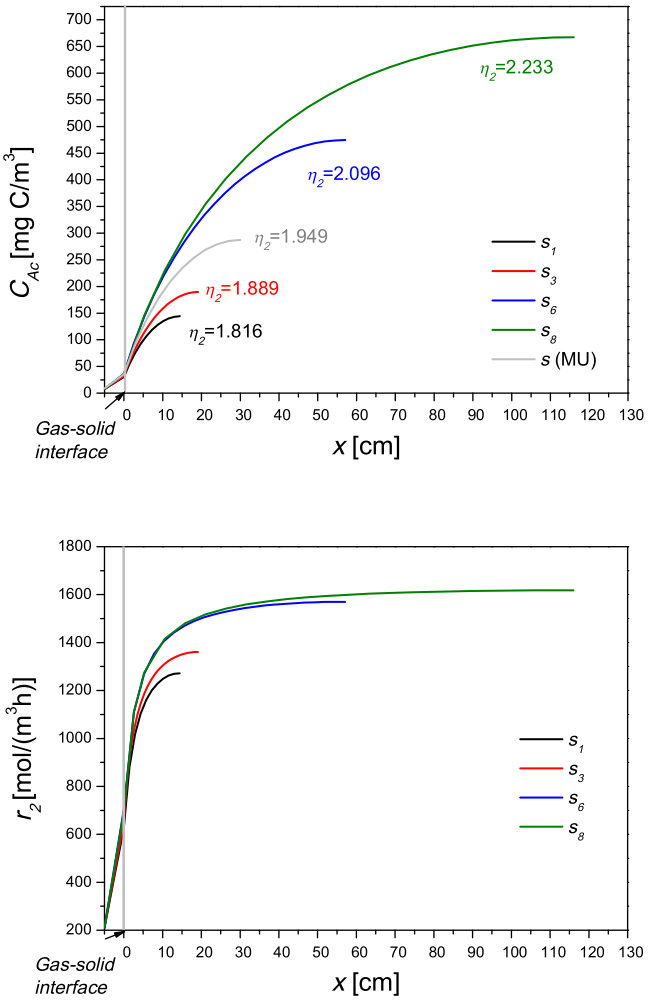

Fig. 8. a) Acetaldehyde concentration cross-section profiles for R_{CN} = 0.5 at z = 0.001 cm, b) reaction rate 2 (r_2) cross-section profiles for R_{CN} = 0.5 at z = 0.001 cm for the conditions of Fig. 2.

Thus, η_2 varies from 1.816 for s_1 to 2.233 for s_8, resulting in an averaged value $\overline{\eta}_2$ = 2.1.

As before, the averaged internal effectiveness factor of reaction 2 is strongly affected by the weight factors of the slices near the corner, which shows the higher relative areas. Fig. 8a also shows the acetaldehyde concentration cross-section profile corresponding to R_{NC} = 0. In this idealized case δ_w = 30 μm is comprised between the thickness of slices s_3 and s_6 for R_{NC} = 0.5, and the concentration profile is located between them.

3.2. Non-uniform coating and thermal effects

To analyse the effect of the non-uniformity of the coating on thermal effects, it is useful to compare the simulation results for two different thermal regimes: adiabatic vs. isothermal. The hypothetical isothermal conditions are represented by making the heat of reactions null in the reactor model. As a common basis of comparison, the same feed flowrate and feed composition (C_{0Et} = 1000 mg C/m^3, $GHSV = 3.06\times10^5$ h^{-1}) are adopted. The inlet temperatures (T_0) are selected to set the outlet composition just in the limit of the environmental specification of VOC emissions (ELV = 20 mg C/m^3). For the isothermal model the ELV is achieved at T_0 = 198.8 °C, while for the adiabatic model the ELV is achieved at T_0 = 179.6 °C (for the idealized case R_{NC} = 0).

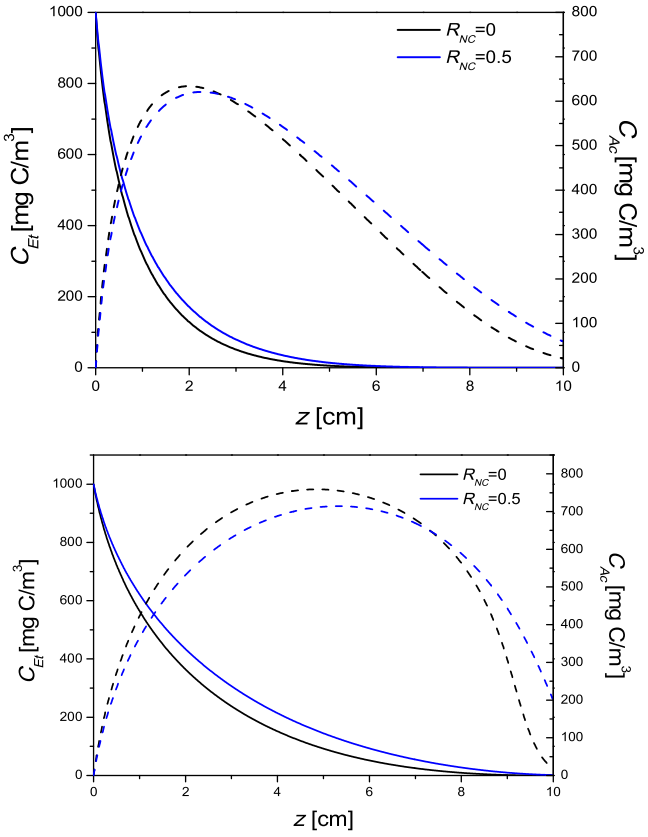

Fig. 9. a) Axial concentration profiles of ethanol and acetaldehyde for the isothermal model for R_{NC} = 0 and 0.5. T_0 = 198.8 °C, C_{0Et} = 1000 mg C/m^3, $GHSV = 3.06\times10^5$ 1/h, $\overline{\delta}_w$ = 30 μm, b = 1.115 mm, L = 10 cm b) Axial concentration profiles of ethanol and acetaldehyde for the adiabatic model for R_{NC} = 0 and 0.5. T_0 = 179.6 °C, C_{0Et} = 1000 mg C/m^3, $GHSV = 3.06\times10^5$ 1/h, $\overline{\delta}_w$ = 30 μm, b = 1.115 mm, L = 10 cm.

Fig. 9a and b shows axial concentration profiles of ethanol and acetaldehyde, respectively, for isothermal and adiabatic models and two different values of the curvature radius (R_{NC} = 0 and 0.5). In the isothermal case (Fig. 9a), the increase in the R_{NC} causes a decrease in the VOC conversion. At the reactor outlet the VOC

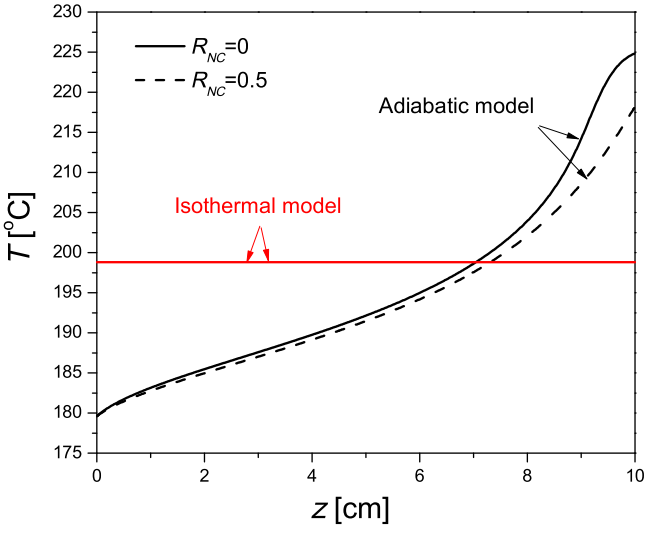

Fig. 10. Axial temperatures profiles in the gas phases for R_{NC} = 0 (continuous line) and R_{NC} = 0.5 (dashed lines), for the isothermal and adiabatic model for the same conditions of Fig. 9a and b.

concentration for R_{NC} = 0.5 (59.1 mg C/m^3) is almost three times higher than that achieved for R_{NC} = 0. For the more realistic adiabatic condition (Fig. 9b), the increase in R_{NC} causes a deeper decrease in the VOC conversion. In fact, the outlet VOC concentration for R_{NC} = 0.5 is now 202.6 mg C/m^3, i.e, the increase in the pollutant emission caused by the washcoat non-uniformity is more than three times that of the isothermal case.

Fig. 10 shows the corresponding temperature profiles for the conditions of Fig. 9. For the isothermal model, a single temperature profile at 198.8 °C represents both situations: R_{NC} = *0* and R_{NC} = 0.5. Conversely, when the model is solved for adiabatic conditions, the total temperature rise in the gas phase for R_{NC} = 0.5 is lower than that of the idealized catalyst distribution. The accumulation of catalytic material in the corner of the channels causes a drop in the effective reaction rates, which leads to lower heat generation rates and therefore lower temperature rises. This thermal effect reinforces the decrease of VOC conversion observed under isothermal conditions. Furthermore, gas-solid temperature gradients also diminish: for R_{NC} = 0, the maximum temperature drop over the film is 3.1 °C, while for R_{NC} = 0.5 the maximum temperature drop is 2.3 °C (results not shown in Figs. 9 and 10). This attenuation in the interfacial temperature gradients also contributes to worsening the emission of VOCs.

3.3. Influence of inlet ethanol concentration (C_{0Et}) under non-uniform coating

Since the feed concentration may fluctuate temporarily in practice (VOC abatement under variable emission patterns) it is important to evaluate the effect of C_{0Et} on the outlet variables when non-uniform catalyst distribution occurs.

Figs. 11–13 illustrate the influence of the inlet ethanol concentration on the reactor behaviour. The results correspond to three different inlet ethanol concentration values (C_{0Et} = 700, 1000 and 1300 mg C/m^3) and two normalized curvature radius (R_{NC} = 0 and 0.5) at constant inlet temperature (T_0 = 180 °C) and constant gas hourly space velocity ($GHSV$ = 3.06 × 10^5 h^{-1}).

As C_{0Et} increases, the intensification of the heat effects (higher ΔT_g inlet-outlet and higher $\Delta T_{s\text{-}g,max}$) causes faster consumption of VOCs for both R_{NC} = 0 and R_{NC} = 0.5. The effect of the catalyst non-uniformity on the pollutant emission, however, will depend on the selected operating condition. For the highest C_{0Et} value, almost complete VOC abatement is achieved in both cases, R_{NC} = 0 and

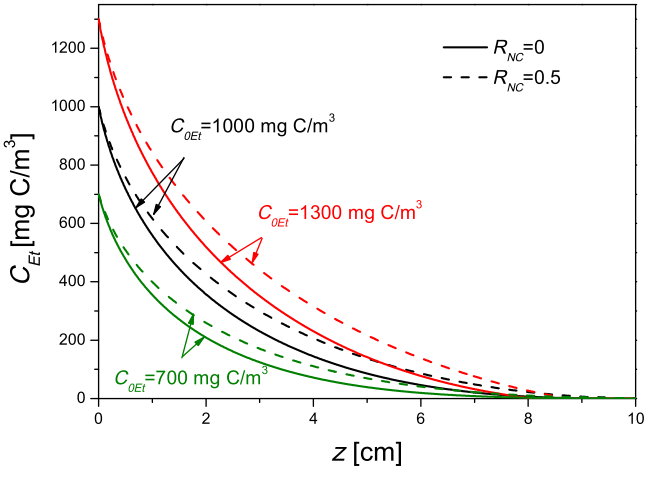

Fig. 11. Axial concentration profiles of ethanol for two curvature normalized radius (R_{NC} = 0 ad 0.5) and three levels of ethanol concentration inlet (C_{0Et} = 700, 1000 and 1300 mg C/m^3). T_0 = 180 °C, $GHSV$ = 3.06 × 10^5 1/h, $\overline{\delta}_w$ = 30 μm, b = 1.115 mm, L = 10 cm.

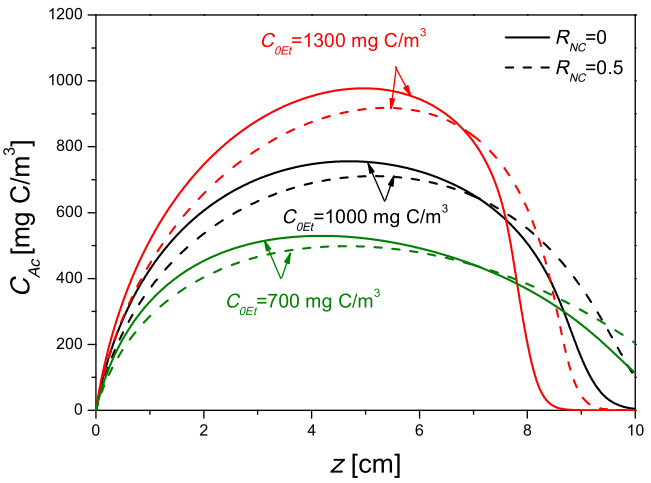

Fig. 12. Axial concentration profiles of acetaldehyde for the same conditions of Fig. 11.

R_{NC} = 0.5. Accordingly, the outlet temperature is the same: 239.7 °C (see Fig. 13, curves for C_{0Et} = 1300 mg C/m^3). However, it is clear that for R_{NC} = 0.5 the complete VOC abatement occurs at an axial position closer to the reactor outlet (Fig. 12).

For C_{0Et} = 1000 mg C/m^3 and R_{NC} = 0 it is possible to ensure the environmental specifications of VOC emission, while for R_{NC} = 0.5 the ELV has been exceeded (Fig. 12). The total temperature rise for R_{NC} = 0.5 is around 5 °C lower than that achieved for R_{NC} = 0 (see Fig. 13). At this intermediate feed concentration, the non-uniformity of the catalyst makes the reactor length insufficient to satisfy the process requirements.

Finally, for the lowest C_{0Et} value it is not possible to accomplish VOC emissions standards in either case. The feed preheating becomes deficient (T_0 excessively low), i.e., even an ideal catalyst distribution (R_{NC} = 0) does not guarantee the fulfilment of the specifications.

3.4. Influence of the inlet temperature (T_0)

Fig. 14 shows the light-off curves for the three levels of ethanol inlet concentration (C_{0Et} = 700, 1000 and 1300 mg C/m^3) and the two values of normalized curvature radius (R_{NC} = 0 and 0.5) selected previously. In the ordinate axis, the variable C_{VOC} represents the concentration of unconverted volatile organic

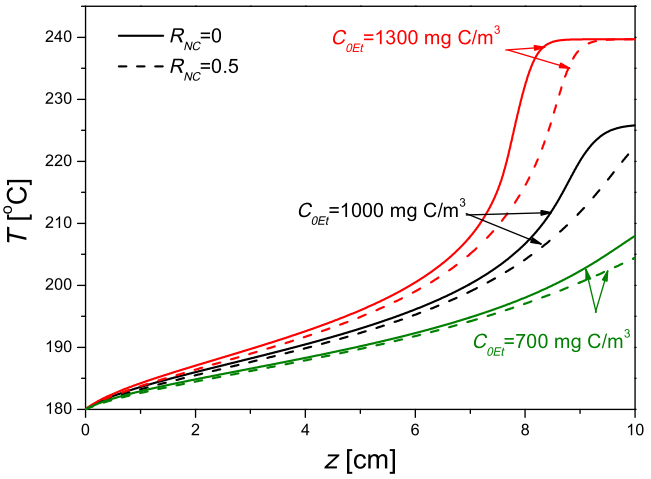

Fig. 13. Axial temperatures profiles in the gas (continuous line) and solid (dashed lines) phases for the same conditions of Fig. 11.

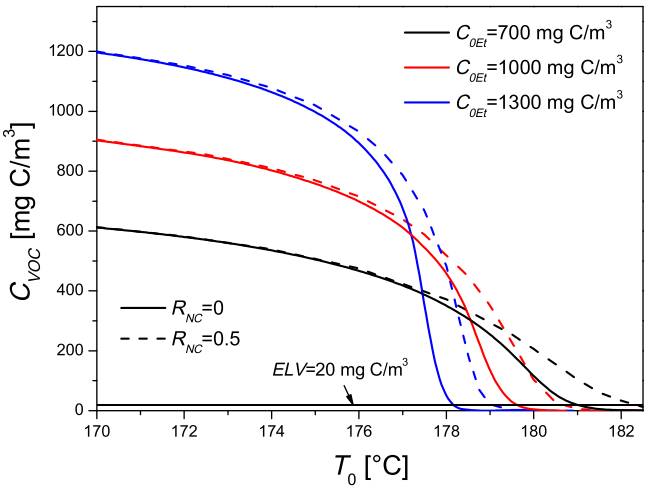

Fig. 14. Influence of the inlet temperature on the outlet concentration of the carbonaceous species (C_{VOC}). Remaining conditions are the same as in Fig. 11.

compounds (ethanol + acetaldehyde) at the reactor outlet. As C_{0Et} increases, light-off curves are steeper due to the higher thermal effects and lower inlet temperatures are needed to reach the *ELV* of VOC. For the idealized case (R_{NC} = 0), the feed stream has to be preheated (at least) up to 181, 179.5 and 178 °C to satisfy the *ELV*, as the feed concentration raises from 700 to 1300 mg C/m^3. This behaviour has been discussed in a previous contribution [36]. It is important to note that as C_{0Et} increases the light-off curves for both normalized curvature radius (R_{NC} = 0 and 0.5) tend to distance themselves from each other. For C_{0Et} = 1300 mg C/m^3, the highest difference in C_{VOC} between both catalyst distribution is registered at T_0 = 178 °C (ΔC_{VOC} = 442 mg C/m^3). This maximum difference is around 228 mg C/m^3 for C_{0Et} = 1000 mg C/m^3 (at T_0 = 179.2 °C) and finally, ΔC_{VOC} = 105 mg C/m^3 for C_{0Et} = 700 mg C/m^3 (at T_0 = 180.7 °C).

Consequently, as the thermal effects are more significant, the non-uniformity of the catalyst coating has a stronger influence on the outlet conversion of VOCs. The common model assumption of ideal catalytic material distribution (R_{NC} = 0) can lead to predict VOC concentrations significantly lower than the real ones.

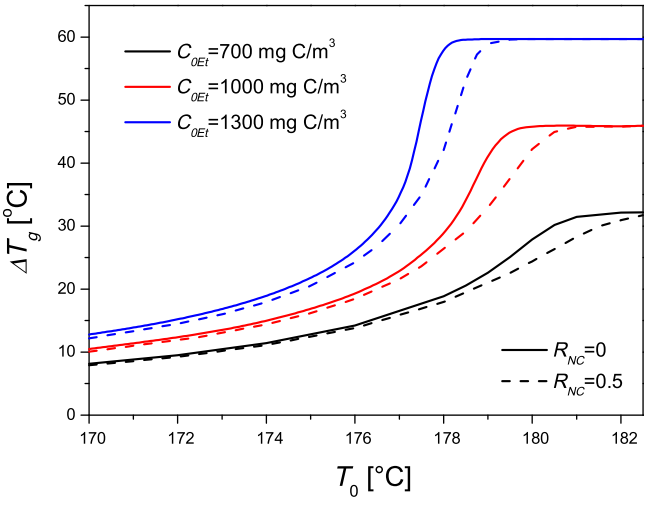

Fig. 15. Influence of the inlet temperature on the total temperature rise in the gas phase. Remaining conditions are the same as in Fig. 11.

The corresponding total temperature rises (ΔT_g) in gas phase are shown in Fig. 15. It is clear that once T_0 is high enough to reach the ELV, ΔT_g becomes constant at the value of the adiabatic temperature rise (ΔT_{ad} = 32.1, 46.1, 59.9 °C for C_{0Et} = 700, 1000 and 1300 mg C/m^3, respectively). Again, as the feed concentration rises, the differences between the curves of ΔT_g corresponding to both curvature radius becomes more pronounced. Under these conditions, the temperature of the gas stream leaving the monolith can be considerably overestimated if R_{NC} = 0 is assumed.

4. Conclusions

A steady-state 1-D heterogeneous mathematical model is used to evaluate the influence of the catalyst distribution inside the channels on the performance of a monolith for VOCs abatement.

The accumulation of catalytic material in the corners of the channels, estimated by the curvature radius (R_{NC}), can deteriorate significantly the reaction rates inside the washcoat. For higher values of R_{NC}, the averaged effectiveness factors drop significantly, leading to conditions of incomplete VOC conversion.

In presence of high feed concentrations of VOCs, the temperature rises are significant, which magnify the effect of the non-uniformity in the catalytic material. As R_{NC} increases, the lower heat generation rates cause lower temperature levels along the reactor length. This result, together with the lower temperature differences in the gas-solid interface, contributes to reduce the effective reaction rates. Consequently, higher inlet temperatures and/or lower space velocities will be necessary to reach the Emission Limit Value of VOC (*ELV* = 20 mg C/m3).

The light-off curves are strongly affected by the value of the curvature radius, i.e, if the catalyst accumulation phenomenon is neglected the differences in the predictions of the unconverted VOCs concentrations can be significant.

The usual modelling assumption of ideal catalytic material distribution (R_{NC} = 0) can result in predicting VOC conversions and outlet gas temperatures higher than the real ones. This overestimation in the outlet variables is clearly non-conservative and may lead to unsuitable designs of the monolith reactor and the preheating zone of the gas stream.

The present simulation results, obtained for an adiabatic catalytic reactor operating at steady-state conditions and for a single pollutant (ethanol) in the feed stream, can be useful for further investigations focused on non-adiabatic monoliths, multiple reactants and/or transient conditions caused by variable emission patterns of VOCs.

Acknowledgements

Support of this work through Universidad Nacional de San Luis (UNSL), Universidad Nacional del Sur (UNS), Agencia Nacional de Promoción Científica y Tecnológica (ANPCyT) and Consejo Nacional de Investigaciones Científicas y Tecnológicas (CONICET) is fully acknowledged.

References

[1] K. Everaert, J. Baeyens, Catalytic combustion of volatile organic compounds, J. Hazard. Mater. B 109 (2004) 113–139.
[2] European Commission. http://ec.europa.eu/environment/air/legis.htm. (Accessed 15 August 2016).
[3] United States Environmental Protection Agency (EPA), 2014. The Clean Air Act. http://www.epw.senate.gov/envlaws/cleanair.pdf. (Accessed 15 August 2016).
[4] F.I. Khan, A.K. Ghoshal, Removal of volatile organic compounds from polluted air, J. Loss Prev. Process Ind. 13 (2000) 527–545.
[5] A. Cybulski, J.A. Moulijn (Eds.), Structured Catalysts and Reactors, second ed., CRC Press – Taylor & Francis Group, Florida, USA, 2006.

[6] X. Wang, R. Daniels, R.W. Bake, Recovery of VOCs from high-volume, low VOC-concentration air streams, AIChE J. 47 (2001) 1094–1100.
[7] G. Ertl, H. Knözinger, F. Schüth, J. Weitkamp, Handbook of Heterogeneous Catalysis, second ed., Wiley-VCH, Weinheim, 2008.
[8] A. Holmgren, B. Andersson, Mass transfer in monolith catalysts-CO oxidation experiments and simulations, Chem. Eng. Sci. 53 (1998) 2285–2298.
[9] A. Kołodzieja, J. Łojewskab, Optimization of structured catalyst carriers for VOC combustion, Catal. Today 105 (2005) 378–384.
[10] R.M. Heck, S. Gulati, R.J. Farrauto, The application of monoliths for gas phase catalytic reactions, Chem. Eng. J. 82 (2001) 149–156.
[11] W.B. Li, J.X. Wang, H. Gong, Catalytic combustion of VOCs on non-noble metal catalysts, Catal. Today 148 (2009) 81–87.
[12] M.R. Morales, B.P. Barbero, L.E. Cadús, Evaluation and characterization of Mn-Cu mixed oxide catalysts for ethanol total oxidation: influence of copper content, Fuel 87 (2008) 1177–1186.
[13] F.N. Agüero, M.R. Morales, F. Duran, B.P. Barbero, L.E. Cadús, MnCu/Cordierite monolith used for catalytic combustion of volatile organic compounds, Chem. Eng. Tech. 36 (2013) 1749–1754.
[14] R.E. Hayes, B. Liu, M. Votsmeier, Calculating effectiveness factors in non-uniform washcoat shapes, Chem. Eng. Sci. 60 (2005) 2037–2050.
[15] R.E. Hayes, S.T. Kolaczkowski, Mass and heat transfer effects in catalytic monolith reactors, Chem. Eng. Sci. 49 (1994) 3587–3599.
[16] D. Papadias, L. Edsberg, P. Björnbom, Simplified method of effectiveness factor calculations for irregular geometries of washcoats, Chem. Eng. Sci. 55 (2000) 1447–1459.
[17] C. Chou, W.E. Stewart, Influence of coating geometry on the effectiveness of monolithic reactors, Chem. Eng. Sci. 41 (1986) 202–204.
[18] D. Leung, R.E. Hayes, S.T. Kolaczkowski, Diffusion limitation in the washcoat of a catalytic monolith reactor, Can. J. Chem. Eng. 74 (1996) 94–103.
[19] S.T. Kolaczkowski, S. Serbetcioglu, Development of combustion catalysts for monolith reactors: a consideration of transport limitations, Appl. Catal. A: Gen. 138 (1996) 199–214.
[20] R.E. Hayes, B. Liu, R. Moxom, M. Votsmeier, The effect of washcoat geometry on mass transfer in monolith reactors, Chem. Eng. Sci. 59 (2004) 3169–3181.
[21] R.E. Hayes, B. Liu, M. Votsmeier, Calculating effectiveness factors in non-uniform washcoat shapes, Chem. Eng. Sci. 60 (2005) 2037–2050.
[22] R.E. Hayes, P.K. Mok, J. Mmbaga, M. Votsmeier, A fast approximation method for computing effectiveness factors with non-linear kinetics, Chem. Eng. Sci. 62 (2007) 2209–2215.
[23] R.E. Hayes, S.T. Kolaczkowski, W.J. Thomas, Finite-element model for a catalytic monolith reactor, Comp. Chem. Eng. 16 (1992) 645–657.
[24] A. Cybulski, J.A. Moulijn, Monoliths in heterogeneous catalysis, Catal. Rev. 36 (1994) 179–270.
[25] F.P. Incropera, D.P. DeWitt, T.L. Bergman, A.S. Lavine, Fundamental of Heat and Mass Transfer, Wiley and Sons, New York, 2001, pp. 260.
[26] F. Kapteijn, G.B. Marin, J.A. Moulijn, Catalytic reaction engineering, chapter 8, in: R.A. van Santen, P.W.N.M. van Leeuwen, J.A. Moulijn, B.A. Averill (Eds.), Catalysis: An Integrated Approach, Elsevier, Amsterdam, 1999, pp. 408.
[27] R.E. Hayes, S.T. Kolaczkowski, Introduction to Catalytic Combustion, first ed., Gordon and Breach Science Publishers, Netherlands, 1997.
[28] M.A. Campesi, N.J. Mariani, M.C. Pramparo, B.P. Barbero, L.E. Cadús, O.M. Martínez, G.F. Barreto, Combustion of volatile organic compounds on a MnCu catalyst: a kinetic study, Cat. Today 176 (2011) 225.
[29] J.M. Smith, H.C. Van Ness, M.M. Abbott, Introduction to Chemical Engineering Thermodynamics, McGraw-Hill, New York, 2005.
[30] M.A. Campesi, Estudio De Sistemas Combinados De Combustión Catalítica De VOCs, Universidad Nacional de La Plata, Argentina, 2012. PhD Thesis http://sedici.unlp.edu.ar/bitstream/handle/10915/27082/Documento_completo.pdf?sequence=1.
[31] R.C. Reid, J.M. Prausnitz, T.K. Sherwood, The Properties of Gases and Liquids, third ed., Mc Graw Hill, New York, 1977.
[32] R.D. Hawthorn, Afterburner catalysis—effects of heat and mass transfer between gas and catalyst surface, AIChE Symp. Ser. 70 (1974) 428–438.
[33] E.N. Fuller, P.D. Schettler, J.C. Giddings, New method for prediction of binary gas-phase diffusion coefficients, Ind. Eng. Chem. 58 (1966) 19–27.
[34] G.F. Froment, K.B. Bischoff, Chemical Reactor Analysis and Design, second ed., Wiley, Toronto, Canada, 1990.
[35] L.F. Shampine, C.W. Gear, A users view of solving stiff ordinary differential equations, SIAM Rev. 21 (1979) 1–17.
[36] M.L. Rodríguez, L.E. Cadús, D.O. Borio, VOCs abatement in adiabatic monolithic reactors: heat effects, transport limitations and design considerations, Chem. Eng. J. 306 (2016) 86–98.